

Tensor and vector spin observables in p-d elastic scattering at 600, 800, and 1000 MeV

M. Haji-Saied,* E. Bleszynski, M. Bleszynski, J. Carroll, G. J. Igo, T. Jaroszewicz, and A. T. M. Wang
Physics Department, University of California at Los Angeles, Los Angeles, California 90024

A. Sagle

Lawrence Berkeley Laboratory, Berkeley, California 94720

J. B. McClelland and C. L. Morris

Los Alamos National Laboratory, Los Alamos, New Mexico 87545

R. Klem

Argonne National Laboratory, Argonne, Illinois 60429

T. Joyce, Y. Makdishi,[†] M. Marshak, B. Mossberg, E. A. Peterson,
 K. Ruddick, and J. Whittaker

Department of Physics, University of Minnesota, Minneapolis, Minnesota 55455

(Received 11 May 1987)

Measurements of the tensor and vector spin observables $C(0,NN,0,0)$, $C(0,SS,0,0)$, and $C(0,N,0,0)$, in p-d elastic scattering at 600, 800, and 1000 MeV equivalent proton bombarding energy, are reported. The data were taken in the range $0.1 < -t < 1.2$ (GeV/c)². The experiment employed a polarized deuteron beam with tensor and vector components of ± 0.75 and ± 0.25 , respectively, a liquid hydrogen target, and a single arm magnetic spectrometer. The tensor and vector spin parameters $C(0,N,0,0)$ and $C(0,NN,0,0)$ were extracted from the data with beam polarization normal to the scattering plane. The observable $C(0,SS,0,0)$ was obtained by precessing the deuteron polarization into the scattering plane. Comparison of the data with the predictions of a relativistic multiple scattering theory is made.

I. INTRODUCTION

A considerable amount of proton-deuteron elastic scattering data at intermediate energies has been accumulated by now.¹⁻⁵ A principal objective of these measurements^{1,3,4} is to obtain complete information on the collision matrix describing this fundamental three-nucleon reaction. Detailed information on the 12 spin amplitudes⁶ describing p-d elastic scattering will be helpful in studies of various theoretical aspects of medium energy nuclear reactions. An interesting application of the data is to establish to what extent p-d elastic scattering data can be explained in terms of the multiple scattering theory employing only two-body NN interactions. An analysis of this type may be carried out in the near future, in view of recent progress made in the measurements of the spin dependence of the nucleon-nucleon (NN) cross sections, and in the amplitude analysis of this data. At the present time, phase shifts for *both* proton-proton *and* proton-neutron scattering appear to be well established up to ~ 500 MeV laboratory kinetic energy.⁷⁻⁹ Therefore, the role of proton-deuteron scattering is now not so much to provide information on NN scattering, but rather to study phenomena specific to few- and many-nucleon systems. Indeed, important information on these phenomena can be extracted from spin observables in p-d elastic scattering at sufficiently large momentum transfers for which multiple scattering

dominates.¹⁰ Calculations of spin-observables in p-d elastic scattering presented in Refs. 10 and 1 were made within the framework of a new multiple scattering model based on the insight into the physical mechanism underlying the nuclear relativistic phenomena.¹¹ The results of these calculations indicate that good agreement between experimental data and the theoretical predictions can be obtained by introducing additional effective contact interactions, which can be interpreted as three-nucleon forces.¹⁰ Previous and planned experiments in p-d elastic scattering at several energies in the range 500–1000 MeV will be used in the future in establishing constraints on these contact interactions.

In the present paper we report on measurements of the deuteron vector, $C(0,N,0,0) \equiv P_y$, and tensor, $C(0,NN,0,0) \equiv P_{yy}$ and $C(0,SS,0,0) \equiv P_{xx}$, spin observables for 600, 800, and 1000 MeV equivalent proton laboratory energy at momentum transfers squared in the range $0.1 < -t < 1.2$ (GeV/c)². The alternate notation of spin observables in terms of parameters P_i , $i=y,xx,yy$, is defined in Ref. 6, and has been used in previous short communications^{3,4} in which the data at 800 and 1000 MeV were reported together with the theoretical interpretation based on the approach of Ref. 6.

The experiment has been performed at the Argonne National Laboratory at the Zero-Gradient Synchrotron (ZGS) facility. The experimental equipment available made it possible to measure tensor and vector spin ob-

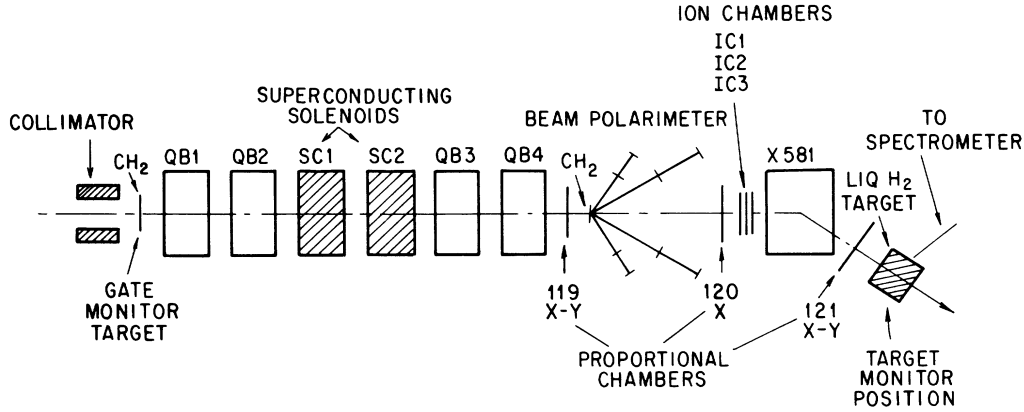


FIG. 1. A schematic view of the beam line, showing the locations of the beam monitors, superconducting solenoids, beam line magnets, beam polarimeter, and liquid hydrogen target.

servables with relatively high precision.^{12,3,4}

In Sec. II of this paper we report that the experimental method used to measure the tensor and vector analyzing powers; in Sec. III the data obtained at deuteron beam energies of 1.2, 1.6, and 2.0 GeV; and, in Sec. IV, comparison of the data with the theoretical predictions based on the recently developed relativistic multiple scattering model¹ is described.

II. EXPERIMENTAL SETUP

The experiment used polarized deuteron beams with momenta $p_d = 3.43, 2.93,$ and 2.43 GeV/c. These were produced at the Argonne ZGS with tensor and vector components oriented along the \hat{y} axis in our coordinate system, normal to the scattering plane. Following the Madison convention¹³ we use the Cartesian frame of reference formed by three orthogonal directions ($\hat{S} \equiv \hat{x}$, $\hat{N} \equiv \hat{y}$, $\hat{L} \equiv \hat{z}$). Here \hat{L} is along the direction of the incident beam momentum \mathbf{k}_i , \hat{N} is normal to the scattering plane $\mathbf{k}_i \times \mathbf{k}_f$, \mathbf{k}_f being the scattered beam momen-

tum, and \hat{S} axis completes a right-handed Cartesian coordinate system. By utilizing a pair of superconducting solenoids in the beam line (see Fig. 1), these components could be precessed into the scattering plane along the \hat{x} axis normal to the beam direction (\hat{z} axis). In either case a four pulse sequence [rate $\sim (3.5 \text{ s})^{-1}$ and width ~ 1 s] with the polarization components $(-p_y, +p_{yy})$, $(-p_y, -p_{yy})$, $(+p_y, -p_{yy})$, $(+p_y, +p_{yy})$ along the y axis were used in the experiment. Here p_y is the magnitude of the vector polarization, and p_{yy} is the magnitude of the tensor polarization of the deuteron. With the superconducting solenoids in the beam line on, the same pattern could be reproduced in the xz plane. The beam intensity varied between 10^8 and 3×10^9 deuterons per pulse. The target was a 10 cm flask containing liquid hydrogen. The direction, position, and emittance of the incident beam were monitored by two x - y and two x multiwire proportional counters read out in an integrated mode (see Figs. 1 and 2). These chambers had a wire spacing of 2 mm. The four position measurements fixed the beam trajectory independently of the bend an-

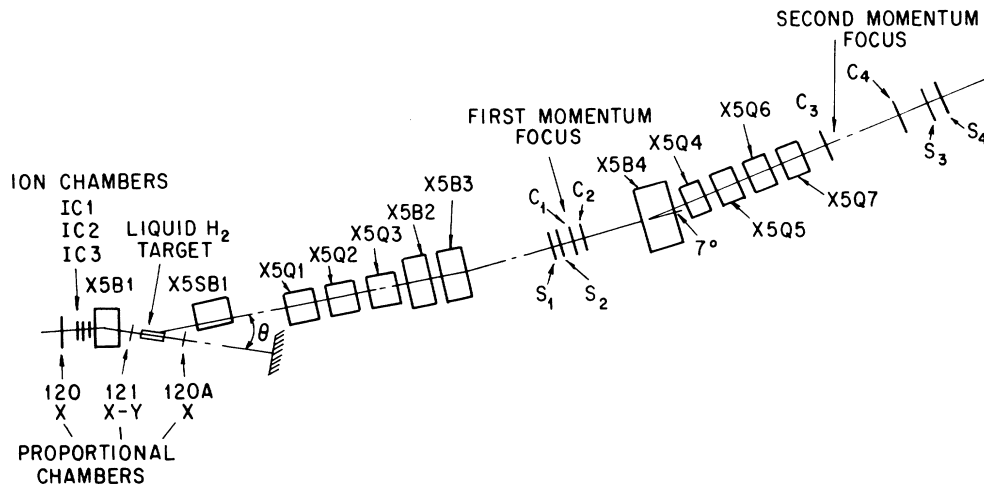


FIG. 2. A schematic view of the spectrometer, showing locations of the various detectors, wire chambers (C_1 – C_4), scintillator counters (S_1 – S_4), and the spectrometer dipoles, quadrupoles and the liquid hydrogen target.

gle in magnet X5B1. The data from the proportional chambers were used to correct the nominal scattering angle. The relative beam intensity was monitored, independent of the spin orientation by three ion chambers, IC1, IC2, and IC3 (see Fig. 1), located just upstream of the magnet X5B1. These tracked to within 3% during the experiment. The intensity of the incident beam was also monitored by a three-scintillation counter telescope located in the vertical plane. This telescope, called the gate monitor, accepted particles scattered from a thin polyethylene target, much larger in dimension than the beam, which was located about 5 m upstream of the liquid hydrogen target. A similar telescope was located vertically under the liquid hydrogen target and is called the target monitor. The spectrometer used in this experiment is shown in Fig. 2. In the first stage, four dipole magnets provide momentum dispersion and bent the spectrometer axis away from the primary beam line; three quadrupole magnets created a spatial focus about 15 m downstream of the target. The second stage used a 2 m dipole with a 7° bend and two pairs of quadrupoles with equal gradients in each member of the pair to form a second focus. In order to achieve the large laboratory scattering angles, the incident beam was bent by dipole magnet X5B1 by as much as 28.7° from its nominal axis to increase the angle between the incident beam and the scattered particles entering the spectrometer. The liquid hydrogen target was moved under remote control to intercept the beam in its new position. The scattered deuterons were steered down the spectrometer axis by septum magnet X5SB1, which was also remotely movable. At the smallest laboratory scattering angle (about 3.57°), dipole magnet X5B1 was off, the hydrogen target was on the nominal deuteron beam line, and dipole magnet X5SB1 was bending deuteron trajectories to the left, looking downstream. At the largest angles, X5B1 and XtSB1 were both bending to the right and the target was farther to the right of the nominal beam line, all directions looking downstream. In the spectrometer deuterons were detected by two scintillator counters, called S_1 and S_2 , and two multiwire, position-sensitive, gas proportional chambers labeled C_1 and C_2 at the first focus

and by two other scintillator counters, called S_3 and S_4 , and the two chambers similar to C_1 and C_2 , labeled C_3 and C_4 , near the second focus. The entire length of the spectrometer was evacuated, except for the regions where the counters and chambers were situated. The data from S counters (S_1, S_2, S_3, S_4) were used to determine the number of scattered deuterons and to calculate the time of flight which gave information as to particle type. Particle trajectory, scattering angle, and momenta were provided by the four chambers C_1, C_2, C_3 , and C_4 . These chambers were two dimensional with the anode and cathode wires in the same direction but in two parallel planes with a separation of 8 mm and an offset of 4 mm. The construction of these chambers allows them to be used as drift chambers or delay line readout chambers. In this experiment the higher resolution afforded by the drift chamber options was not needed. The chambers were operated with a gas mixture of 20% isobutane, 0.2% freon, and about 80% argon bubbled through isopropyl alcohol. The absolute value of the tensor alignment of the beam was measured using the nuclear reaction ${}^3\text{H}(d,n){}^4\text{He}$ at the source.¹⁴

In order to measure the polarization of the deuteron beam, deuterons are accelerated to an energy approximately 55 keV. Then they impinge on a thick titanium tritide target.¹⁴ Two scintillator detectors oriented at 0° and 90° with respect to the spin quantization axis were used to measure the anisotropy of the neutrons produced in the d-t reactions. The measured anisotropy was used to calculate the tensor alignment. This parameter was measured frequently over the course of the experiment; a total of eleven times. At the beginning the magnitude was 0.84 ± 0.03 , but at the time of the data taking the value of tensor alignment was 0.75 ± 0.03 and was equal for positive and negative values within the uncertainty (± 0.03) and remained so throughout the rest of the experiment. From the source dynamics the absolute value of the vector polarization was also established at the value of 0.25 with the same fractional uncertainty. Relative values of the beam vector polarization were determined with an uncertainty of $\pm 4\%$ by utilizing a thin CH_2 target polarimeter located at the point at which the

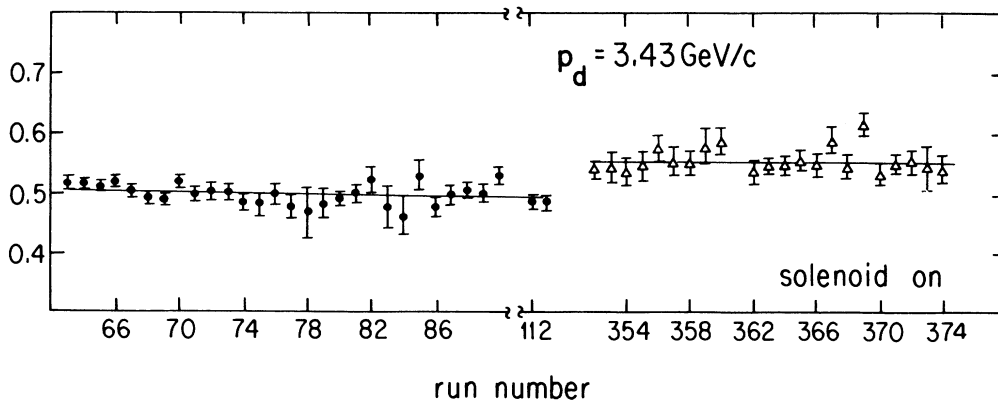


FIG. 3. A typical set of measurements of a quantity proportional to $(P_{yy} - P_{xx})$ from the beam polarimeter at $p_d = 3.43 \text{ GeV}/c$ and $\theta_{\text{lab}} = 9^\circ$. Circles and triangles represent the measurements during two different periods of running time at the same energy. The solid lines display the χ^2 fits assuming a linear relation to the data.

deuterons were extracted from the ZGS. Relative values of the tensor alignment of the beam were measured in another polarimeter, also utilizing a CH_2 target, located upstream of the dipole magnet X5B1 (see Fig. 1). The polarimeter has arms in both the horizontal and vertical planes and left, right, up, and down forward-recoil telescopes identified d-p elastic events. This polarimeter allowed us to measure the asymmetry of the deuteron beam when the beam was polarized perpendicularly to the scattering plane (solenoid off) or when the deuterons were precessed with polarization axis in the scattering plane (solenoid on). The coincidence rates were particularly sensitive to P_{yy} (P_{xx}) and allowed us to measure a numerically large quantity, proportional to $(P_{yy} - P_{xx})$, and thus check the relative beam polarization accurately. Some results of these measurements are shown in Fig. 3. In this figure the circles and triangles represent data taken at the beginning and late in the data taking period. In between the polarimeter was readjusted for other energies. Then the data are fitted by straight lines separately with reduced χ^2 of 1.26 and 1.73, respectively. No depolarization resonances were passed through in the process of the acceleration to the momenta used in this experiment.¹⁵ Depolarization effects are generally expected to be negligible since the deuteron's magnetic moment is one-third as large as that of the proton. No depolarization of the proton beam was found in earlier experiments.^{16,17}

III. DATA COLLECTION AND ANALYSIS

The data collection at each incident energy required 3–4 d. Measurements were done in the order 2.0, 1.2, 1.6, 2.0, and 1.2 GeV. At each incident energy, the angular settings were selected in a somewhat random order; in general, adjacent angles were measured at different times. Events collected at each angle setting of the spectrometer were binned in one or two parts. Chamber data and time-of-flight information from the S counters were written event by event on magnetic tape. Other information, i.e., counts recorded by monitor telescopes and chamber beam polarimeter, and the number of $(S_1 * S_2 * S_3 * S_4)$ coincidents, were also recorded after each beam pulse. In addition, $(S_1 * S_2 * S_3 * S_4)$ coincidences and digitized integrated charge from ion chambers were recorded on visual scalars during the last half of the experiment. Data were also accumulated at selected angles with the target empty. The final data analysis was done off line with the software completely independent of the software used to write data tapes. Some of the analysis had to be done without magnetic tapes (2.0 and 1.6 GeV data) due to tape drive failure. Data obtained in this mode were treated on a pulse to pulse rather than event by event basis. We determined the number of elastically scattered deuterons which passed through the spectrometer for each polarity ($Y_{\uparrow\uparrow}$, $Y_{\downarrow\uparrow}$, $Y_{\uparrow\downarrow}$, $Y_{\downarrow\downarrow}$) and the intensity ($I_{\uparrow\uparrow}$, $I_{\downarrow\uparrow}$, $I_{\uparrow\downarrow}$, $I_{\downarrow\downarrow}$) for each beam pulse [see text below and Eq. (3.2) for definition of notation]. When the magnetic tape unit was operative the scattering angle was reconstructed for each event, using the output of the delay line chambers

and the optical parameters of the spectrometer.¹⁸ These were histogrammed separately for events collected with different incident deuteron polarity. The areas of these histograms were denoted as $Y_{\uparrow\uparrow}$, $Y_{\downarrow\uparrow}$, $Y_{\uparrow\downarrow}$, and $Y_{\downarrow\downarrow}$. For small angle data, it was desirable to divide the data into two angular bins in order to obtain adequate angular resolution in the sharply falling part of the small angle elastic scattering angular distribution.

In this experiment, a polarized deuteron beam is incident on an unpolarized hydrogen target. The corresponding deuteron spin density matrix ρ_i , representing the beam polarized perpendicular to the scattering plane, is

$$\rho_i = (1 \pm \frac{1}{2} p_y \hat{P}_y \pm \frac{1}{2} p_{yy} \hat{P}_{yy}), \quad (3.1)$$

where \hat{P}_y and \hat{P}_{yy} are the deuteron spin and quadrupole moment operators. The differential cross section for the angular distribution of scattered deuterons is

$$\frac{d\sigma}{d\Omega_{\uparrow(\downarrow), \downarrow(\uparrow)}} = \frac{d\sigma}{d\Omega_{\text{unpol}}} (1 \pm \frac{1}{2} p_y P_y + \frac{1}{2} p_{yy} P_{yy}), \quad (3.2)$$

where the upward (downward) pointing arrow (first subscript) indicates the upward (downward) direction of the

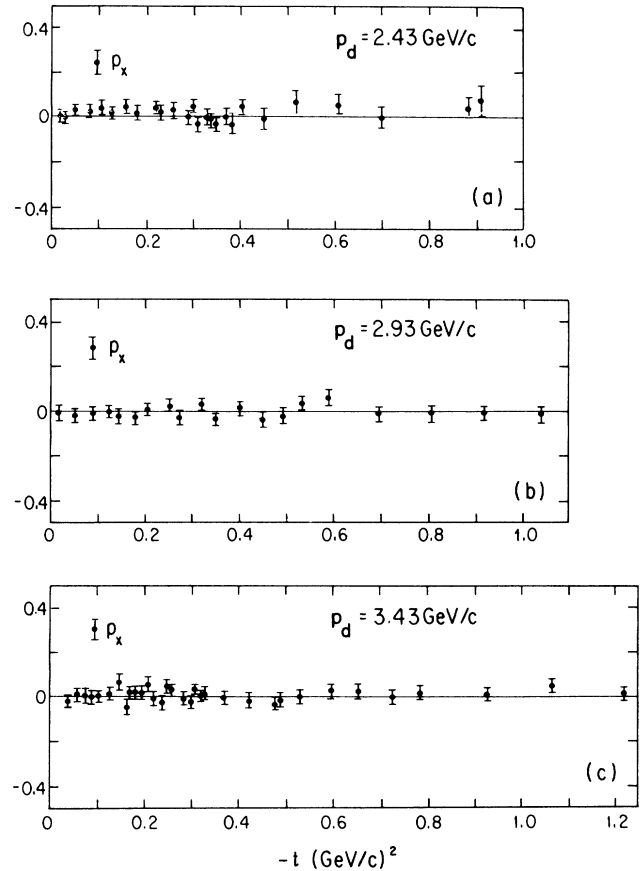


FIG. 4. (a)–(c) Experimental results for the spin observables $C(0, S, 0, 0) \equiv P_x$ at (a) 600 MeV EPBE, (b) 800 MeV EPBE, and (c) 1000 MeV EPBE, which are consistent with zero.

vector polarization and gives rise to plus and minus signs, respectively, for the term proportional to the magnitude, P_y , on the right-hand side, and $d\sigma/d\Omega_{\text{unpol}}$ is the differential cross section which would be measured with an unpolarized deuteron beam. The direction of the arrow in the second subscript indicates the direction of the tensor alignment and is related to the plus and minus signs in the term proportional to P_{yy} . The differential cross section with the solenoid on is, with notation similar to Eq. (3.2), given by

$$\frac{d\sigma}{d\Omega_{\uparrow(1),\downarrow(1)}} = \frac{d\sigma}{d\Omega_{\text{unpol}}} \left(1 \pm \frac{3}{2} p_x P_x + \frac{1}{2} p_{xx} P_{xx} \right). \quad (3.3)$$

In Eqs. (3.1)–(3.3), p_y , p_{yy} , and p_{xx} are the components of the beam's polarization, and P_y , P_x , P_{yy} , and P_{xx} are the Cartesian components of the induced vector and tensor analyzing powers, respectively.⁶ Since p_x is in the scattering plane, P_x will vanish due to parity invariance. Thus the measurements obtained for P_x [see Fig. 4(a)–4(c)], which are consistent with zero, provide a check on the data. The tensor and vector observables may be expressed in terms of the quantities A , B , C , and D , where $A \equiv Y_{\uparrow\uparrow}/I_{\uparrow\uparrow}$, $B \equiv Y_{\downarrow\downarrow}/I_{\downarrow\downarrow}$, $C \equiv Y_{\uparrow\downarrow}/I_{\uparrow\downarrow}$, and $D \equiv Y_{\downarrow\uparrow}/I_{\downarrow\uparrow}$, are extracted from the measured yields ($Y_{\uparrow\uparrow}$, $Y_{\downarrow\downarrow}$, $Y_{\uparrow\downarrow}$, $Y_{\downarrow\uparrow}$) and beam fluxes ($I_{\uparrow\uparrow}$, $I_{\downarrow\downarrow}$, $I_{\uparrow\downarrow}$, $I_{\downarrow\uparrow}$). In terms of A , B , C , and D the deuteron tensor observables are

$$\frac{1}{2} p_{yy} P_{yy} = \frac{(A+B)-(C+D)}{(A+B)-(C+D)}, \quad (3.4a)$$

$$\frac{3}{2} p_y P_y = \frac{(A+C)-(B+D)}{(A+C)-(B+D)}, \quad (3.4b)$$

with the solenoid off, and

$$\frac{1}{2} p_{xx} P_{xx} = \frac{(A+B)-(C+D)}{(A+B)-(C+D)}, \quad (3.4c)$$

$$\frac{3}{2} p_x P_x = \frac{(A+C)-(B+D)}{(A+C)-(B+D)}, \quad (3.4d)$$

with the solenoid on. The deuterons scattered from the empty target flask and surrounding environment contribute to the measured asymmetries. The background contribution to the measured asymmetries was calculated for those runs which had corresponding target empty runs. There were numerous enough and representative enough so that they could be used to evaluate and correct the effect of the target flask and surrounding environment for all measurements. The results are presented in Figs. 4–7. The errors include background as well as statistical sources of error. Additional sources of error due to systematics are believed to be small relative to the statistical errors because of the ratio method employed to calculate the asymmetries and because the method used to obtain the data [sequential pulses with systematically varying polarization direction tend to average out long term (> 12 s) drifts in chamber efficiencies, electronic drifts, deteriorating beam polarization, etc.]. The induced vector polarization P_y and tensor components P_{yy} and P_{xx} , extracted from the asymmetry measurements at 2 GeV (3.43 GeV/c, 1 GeV EPBE), at 1.6 GeV (2.93 GeV/c, 0.8 GeV EPBE), and at

1.2 GeV (2.43 GeV/c, 0.6 GeV EPBE) are shown in Figs. 5–7. The notation EPBE means “equivalent proton bombarding energy.”

IV. THEORETICAL ANALYSIS

We have chosen to compare our data with the theoretical predictions of the recently developed relativistic multiple scattering model of Ref. 1. Within the framework of this approach the p-d scattering amplitude is assumed, analogously as in the Glauber theory, to be given

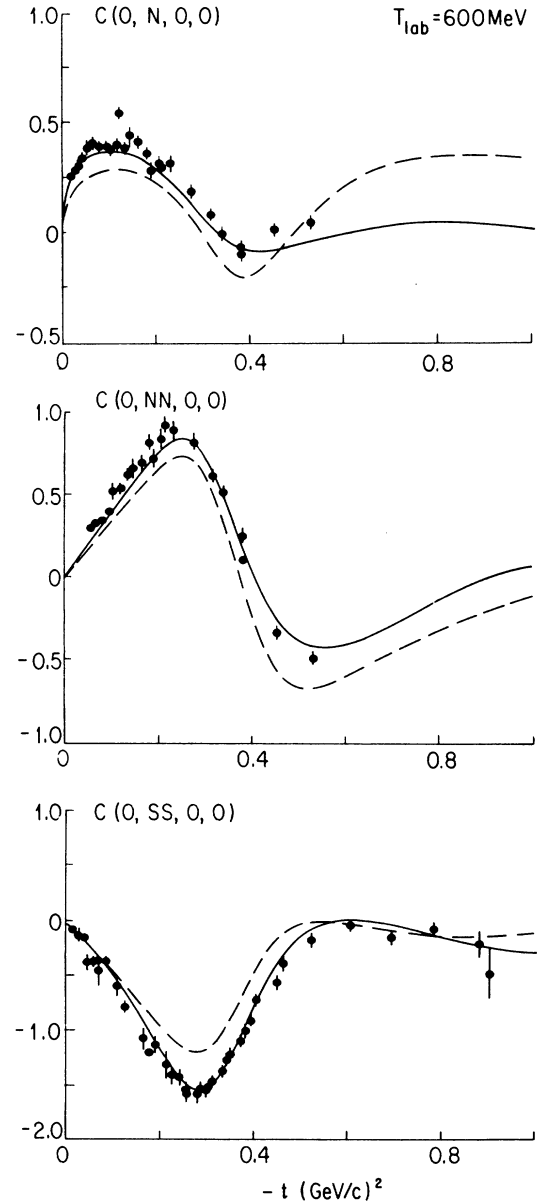


FIG. 5. Experimental results for the spin observables $C(0, N, 0, 0)$, $C(0, NN, 0, 0)$, and $C(0, SS, 0, 0)$ at 600 MeV EPBE. The solid and dashed lines represent theoretical calculations described in the text.

as a sum of subamplitudes F_s and F_d representing single and double collision processes,

$$F_{pd} = F_s + F_d . \quad (4.1)$$

The subamplitudes F_s and F_d are then expressed in terms of fully-spin-dependent amplitudes describing projectile-target neutron and projectile-target proton interactions, and in terms of the S - and D -wave components of the deuteron wave function. The method of calculating the single collision amplitude F_s is identical

with that of Ref. 6. The double collision term, however, is obtained by using a relativistic representation of the NN scattering amplitudes and the relativistic Dirac propagator of the projectile. With these assumptions the transition amplitude for the double collision process involves the integral over the proton three momentum \mathbf{p} in the intermediate state of the expression:

$$[F_{NN}^0 + (\tau_1 \cdot \tau) F_{NN}^1] \frac{1}{\not{p} - m} [F_{NN}^0 + (\tau_2 \cdot \tau) F_{NN}^1] , \quad (4.2)$$

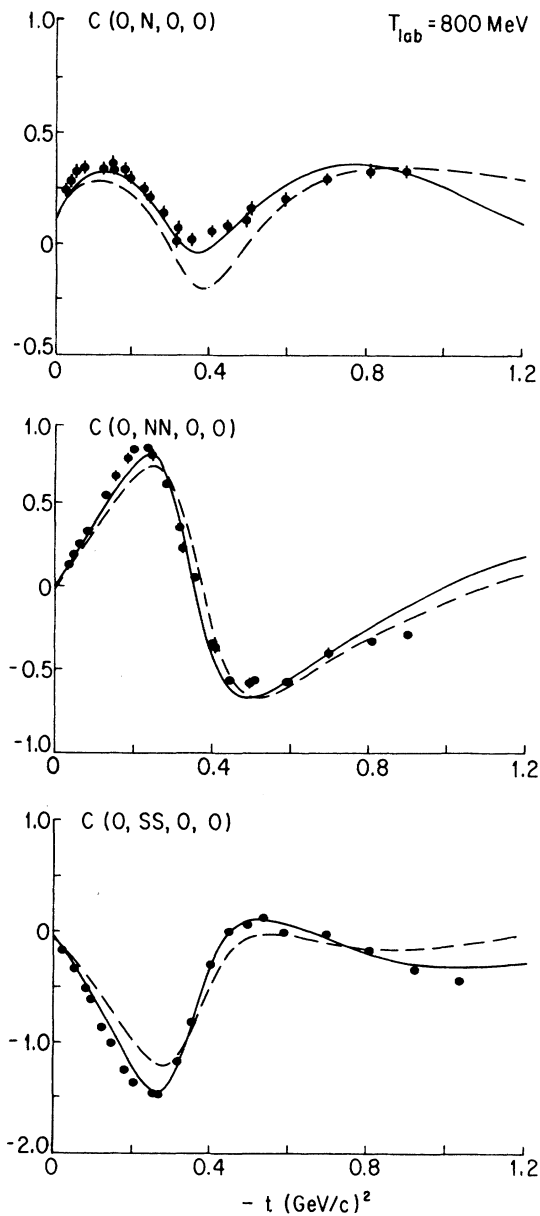


FIG. 6. Experimental results for the spin observables $C(0, N, 0, 0)$, $C(0, NN, 0, 0)$, and $C(0, SS, 0, 0)$ at 800 MeV EPBE. The solid and dashed lines represent theoretical calculations described in the text.

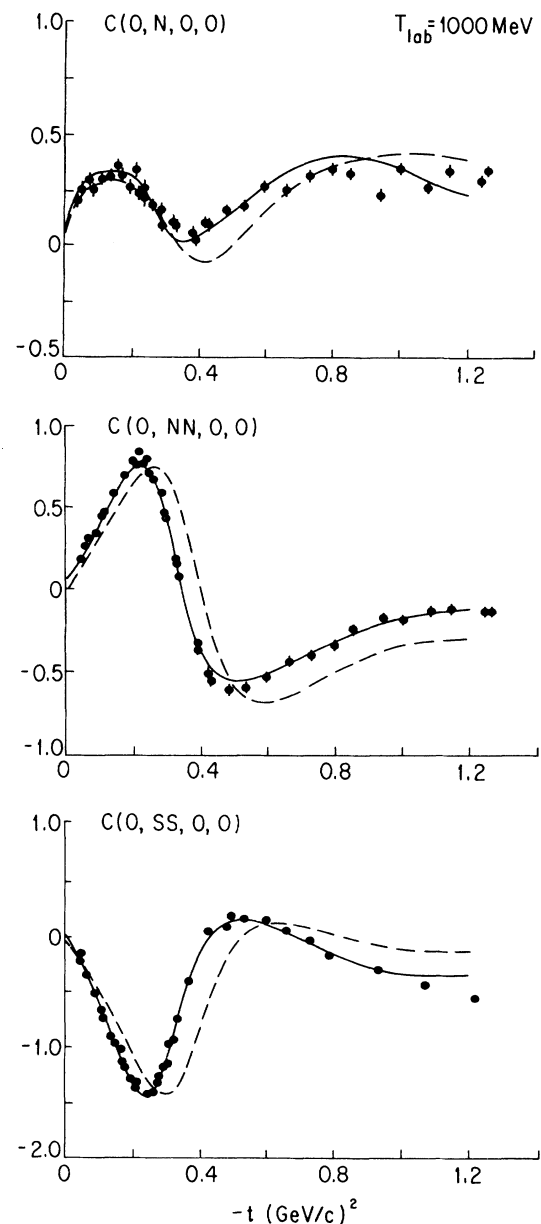


FIG. 7. Experimental results for the spin observables $C(0, N, 0, 0)$, $C(0, NN, 0, 0)$, and $C(0, SS, 0, 0)$ at 1000 MeV EPBE. The solid and dashed lines represent theoretical calculations described in the text.

where τ , τ_1 , and τ_2 are the isospin operators of the projectile and two target nucleons, respectively. The isoscalar $F_{\text{NN}}^{I=0}$ and isovector $F_{\text{NN}}^{I=1}$ components of the relativistic NN amplitude is parametrized as¹

$$F_{\text{NN}}^I(\mathbf{p}', \mathbf{p}) = \sum_{j=1}^5 \left[1 + \xi_j^I \frac{\not{p}' - m}{2m} \right] O_j F_j^I(s, t) \times \left[1 + \xi_j^I \frac{\not{p} - m}{2m} \right], \quad (4.3)$$

p and p' being the initial and final projectile nucleon momenta. Here O_j , $j = 1, 5$, are linearly independent operators acting in the four dimensional Dirac spaces of the projectile (nucleon 1) and the target nucleon (nucleon 2). By following the commonly used representation^{19,20} we have chosen them as scalar, vector, tensor, pseudoscalar, and axial operators: $O_j = 1$, $\gamma(1) \cdot \gamma(2)$, $\sigma(1)_{\nu\mu} \sigma(2)^{\nu\mu}$, $\gamma(1)_5 \gamma(1)_{\mu} \gamma(2)_5 \gamma(2)^{\mu}$, and $\gamma(1)_5 \gamma(2)_5$.

The subamplitudes F_j^I , $j = 1, \dots, 5$, are functions of the usual Lorentz scalars, t and s . The on-mass-shell parts of the amplitudes F_j^I can be determined (up to an arbitrary phase factor) by requiring consistency with a phase shift analysis of NN scattering data. Terms involving ξ_j^I do not contribute to the on-mass-shell NN scattering, but do contribute to the double collision term in which the integration over the intermediate projectile momentum covers all (on-mass-shell and off-mass-shell) values. Each term $\xi_j^I(\not{p} - m)$ entering into the expression for F_{NN}^I generates in the double scattering amplitude [see Eq. (4.2)] a nonpole term which can be interpreted as a three-body contact interaction.¹ Physically, contact interactions represent effects of nucleon compositeness and of nonlocal meson-nucleon couplings.¹¹ The projectile is treated as a relativistic spin- $\frac{1}{2}$ Dirac particle, while the motions of the target nucleons are assumed to be sufficiently slow to be described by nonrelativistic wave functions. More precisely, in Eq. (4.3) we keep only the zeroth and first order terms in the q/m expansion of the NN amplitude and the target wave function. Here q is the momentum transfer and m is the nucleon mass. In order to carry out calculations with a nonrelativistic target wave function, the relativistic nucleon-nucleon F_{NN}^I amplitudes have been reduced to a nonrelativistic 2×2 matrix form in the space of states of the target nucleons. This two component reduction of F_{NN}^I has

been carried out by evaluating the matrix element of the operators F^I between the positive energy Dirac spinors of the target nucleon in the target nucleon Breit frame.¹ The target wave function was parametrized in terms of the nonrelativistic Reid soft core potential.²¹ The on-mass-shell NN amplitudes have been obtained from a recent phase shift analysis (solution SM86).⁸

The solid curves and the dashed curves displayed in Figs. 5–7 correspond to two different ways of including contact interactions. The dashed curves were obtained by setting the parameters of the isoscalar part of the amplitude of Eq. (4.3), $\xi_j^0 = 0$. The isovector parameters ξ_j^1 were taken as $\xi_1^1 = \xi_2^1 = \xi_3^1 = \xi_4^1 = 0$ and $\xi_5^1 = 1$. This prescription corresponds to the relativistic impulse approximation of Ref. 19. We note that in the case of elastic scattering of protons from spin zero nuclei only three [(1) isoscalar-scalar, (2) isoscalar-vector, and (3) isoscalar-tensor] out of ten components of the amplitude (4.3) contribute. In our case all ten components contribute. The choice of the parameter $\xi_5^1 = 1$ is consistent with the notion that the component of the NN amplitude associated with this parameter is dominated by a $1-\pi$ exchange mechanism. This choice is equivalent to the replacement of the pseudoscalar coupling with the axial coupling. The solid curves at all energies were obtained by adjusting the parameters ξ_j^1 in order to obtain a best fit to the complete data set. In the fitting process for the 800 MeV case other data for the polarized p-d elastic scattering at 800 MeV were included. These results demonstrate that it is possible to achieve quite good agreement between the theoretical calculations and the data by being consistent with the on-mass-shell NN amplitudes following from a given phase shift analysis. The agreement can be obtained by varying the strengths of the contact interaction terms. However, we should mention that our analysis of the contributions from the contact interactions should be repeated in the future after a unique set of NN phase shift amplitudes are determined. Currently we find quite substantial differences between the parameters of the contact interactions obtained, by using alternate phase shift analysis solutions (SP82 of Arndt,⁸ and that of Bystricky *et al.*⁹). A detailed description of the calculations presented in this paper will be published elsewhere

This work was supported in part by the U.S. Department of Energy.

*Present address: Nuclear Research Center, AEOI, Post Office Box 11385-8486, Tehran, Iran.

†Present address: Brookhaven National Laboratory, AGS, Upton, NY 11973.

¹E. Bleszynski, M. Bleszynski, and T. Jaroszewicz, in *Intersections Between Particle and Nuclear Physics*, Lakehouse, 1986, edited by D. F. Geesaman, AIP Conf. Proc. No. 150 (AIP, New York, 1986), p. 1208, unpublished.

²E. Winkelman *et al.*, Phys. Rev. C **21**, 2535 (1980).

³M. Bleszynski, G. J. Igo, J. Carroll, A. Sagle, C. L. Morris, T.

Joyce, Y. Makdishi, M. Marshak, B. Mossberg, E. A. Peterson, K. Ruddick, and J. Whittaker, Phys. Lett. **87B**, 1978 (1979).

⁴M. Bleszynski, G. J. Igo, J. Carroll, A. Sagle, C. L. Morris, T. Joyce, Y. Makdishi, M. Marshak, B. Mossberg, E. A. Peterson, K. Ruddick, and J. Whittaker, Phys. Lett. **106B**, 42 (1981).

⁵J. Arvieux *et al.*, Nuc. Phys. **A431**, 613 (1984).

⁶G. Alberi, M. Bleszynski and T. Jaroszewicz, Ann. Phys. (N.Y.) **142**, 299 (1982).

- ⁷E. Aprile *et al.*, Phys. Rev. Lett. **46**, 1047 (1983).
- ⁸R. A. Arndt, L. D. Roper, R. A. Bryan, R. B. Clark, B. J. VerWest, and P. Signell, Phys. Rev. D **28**, 97 (1983).
- ⁹J. Bysticky, C. Lechanoine-Leluc, and F. Lehar, Saclay Report DPhPE 86-13, 1986.
- ¹⁰E. Bleszynski, M. Bleszynski, and T. Jaroszewicz, in *Proceedings of the International Symposium on The Three-Body Force in the Three-Nucleon System*, Berlin, 1986, Vol. 482 of *Lecture Notes in Physics*, edited by B. L. Berman and B. F. Gibson (Springer-Verlag, Berlin, 1986).
- ¹¹E. Bleszynski, M. Bleszynski, and T. Jaroszewicz, Phys. Rev. Lett. **28**, 422 (1987).
- ¹²G. J. Igo, M. Bleszynski, J. Carroll, A. Sagle, C. L. Morris, T. Joyce, Y. Makdishi, M. Marshak, B. Mossberg, E. A. Peterson, K. Ruddick, and J. Whittaker, Phys. Rev. Lett. **43**, 425 (1979).
- ¹³G. D. Ohlsen, Rep. Progr. Phys. **35**, 717 (1972).
- ¹⁴F. Seiler, and E. Baumgartner, in *Proceedings of the Third International Symposium on Polarized Phenomena in Nuclear Reactions*, Madison, 1970, edited by H. H. Barschall and W. Haerberli (University of Wisconsin, Madison, 1971), p. 518.
- ¹⁵E. Parker, private communication.
- ¹⁶E. Biegert, J. B. Carroll, W. Dragoset, Jr., R. Klem, L. Lesikar, M. L. Marshak, E. A. Peterson, K. Ruddick, R. Talaga, and A. Wriekat, Phys. Rev. Lett. **41**, 1098 (1978).
- ¹⁷R. D. Klem, G. J. Igo, R. Talaga, A. Wriekat, H. Courant, K. Einsweiler, T. Joyce, H. Kagan, Y. I. Makdishi, M. L. Marshak, B. Mossberg, E. A. Peterson, K. Ruddick, and T. Walsh, Phys. Rev. Lett. **38**, 1272 (1977).
- ¹⁸R. D. Klem, private communication.
- ¹⁹J. A. McNeil, J. R. Shepard, and S. J. Wallace, Phys. Rev. Lett. **50**, 1439 (1983).
- ²⁰M. L. Goldberger, M. T. Grisaru, S. W. MacDowell, and D. Y. Wong, Phys. Rev. **120**, 2250 (1960).
- ²¹W. Reid, Ann. Phys. (N.Y.) **192**, 233 (1982).